AGU PUBLICATIONS

Journal of Advances in Modeling Earth Systems

RESEARCH ARTICLE
10.1002/2013MS000241

Parameterization and sensitivity analysis of a process-based terrestrial ecosystem model using adjoint method

Qing Zhu[1,2] and Qianlai Zhuang[1,2,3]

[1]Purdue Climate Change Research Center, Purdue University, West Lafayette, Indiana, USA, [2]Department of Earth, Atmospheric, and Planetary Sciences, Purdue University, West Lafayette, Indiana, USA, [3]Department of Agronomy, Purdue University, West Lafayette, Indiana, USA

Key Points:
- Develop an adjoint version of process-based biogeochemical model (TEM)
- Conduct sensitivity analysis to rank importance of model parameters
- Constrain TEM by using in situ observational data

Correspondence to:
Q. Zhu,
zhuq@purdue.edu

Citation:
Zhu, Q., and Q. Zhuang (2014), Parameterization and sensitivity analysis of a process-based terrestrial ecosystem model using adjoint method, *J. Adv. Model. Earth Syst.*, *6*, doi:10.1002/2013MS000241.

Received 6 MAY 2013
Accepted 9 MAR 2014
Accepted article online 13 MAR 2014

Abstract We developed an adjoint version of a process-based biogeochemistry model, the Terrestrial Ecosystem Model (TEM). The adjoint model of TEM was then used to: (1) conduct sensitivity studies of net ecosystem production (NEP) for three terrestrial ecosystems: grassland, deciduous broadleaf forest and evergreen needle-leaf forest; (2) rank the importance of parameters in controlling NEP; (3) optimize the model parameters by assimilating eddy flux data of NEP; and (4) evaluate parameterization by extrapolating optimal parameters to other sites that have the same plant functional type as the calibration sites. We found that: (1) the maximum rate of photosynthesis (C_{MAX}) was the most important parameter in determining NEP, while the importance of the remaining parameters varied depending on plant functional type, suggesting that the same ecosystem process has different degrees of importance in modeling carbon fluxes; (2) the sensitivity of NEP to C_{MAX} had a significant seasonal variability and the control of C_{MAX} on NEP was much larger in growing season (defined as from April to October) than that in nongrowing season (defined as from December to March); and (3) after parameterization, TEM could reasonably reproduce carbon fluxes observed at eddy flux tower sites. This study provided an effective model-data fusion framework of TEM, which could improve the future quantification of terrestrial ecosystem carbon fluxes at both site and regional levels.

1. Introduction

Process-based biogeochemical models play an important role in quantifying the dynamics of global carbon and nitrogen [*Cao et al*., 1998; *Limpens et al*., 2008; *McGuire et al*., 2001; *Melillo et al*., 1993; *Thornton et al*., 2007]. Various ecosystem models are developed during recent decades based on different model philosophies, for example, Terrestrial Ecosystem Model (TEM) [*Zhuang et al*., 2003], Biome-BGC [*Running and Hunt*, 1993], Carnegie-Ames Stanford Approach (CASA) [*Potter et al*., 1993], Simple Diagnostic Biosphere Model (SDBM) [*Knorr and Heimann*, 1995], and Biosphere Energy Transfer Hydrology scheme (BETHY) [*Knorr and Heimann*, 2001]. These models have been extensively used to estimate global carbon dynamics. However, their results are inconsistent and highly uncertain. Intercomparison studies of different terrestrial ecosystem models [*Cramer et al*., 1999, 2001; *Henderson-Sellers et al*., 1995; *Morales et al*., 2005; *Schaefer et al*., 2012] show that model structure and model parameters are two major sources of uncertainty in those ecosystem models. Thus, it is fundamentally important to reduce the existing uncertainties in order to reasonably estimate regional and global carbon budgets and improve our understanding of the underlying ecosystem processes. The uncertainty from model structure exists where physical or biogeochemical processes are represented with mathematical equations in the models [*Zaehle et al*., 2005]. By comparing two models that only differ in the representation of a particular process and have an identical representation of any other key biogeochemical processes, the model structure uncertainty can be reduced through optimization [*Smith et al*., 2001]. The uncertainty of model parameters is another major source of simulation biases [*Medlyn et al*., 2005]. Only a limited number of model parameters are measureable. Furthermore, these measured parameters (either from field studies or lab experiments) are usually conditioned on specific geographical location, plant functional type, soil characteristics, and climate condition. Under most circumstances, model parameters are estimated based on prior knowledge and available data [*Luo et al*., 2003; *Knorr and Kattge*, 2005; *Zhu and Zhuang*, 2013a, 2013b, 2013c]. The goodness of the estimated parameters, however, is still restricted to the scarcity of observational data and the limited information within a specific data set [*Luo et al*., 2009]. Thus, how to effectively extract useful information from existing data to constrain the parameter uncertainty becomes a critical issue.

One effective tool to reduce the parameter uncertainties of terrestrial ecosystem models is data assimilation (DA) [*Raupach et al*., 2005; *Williams et al*., 2009; *Luo et al*., 2011], which inversely estimates the unobservable model parameters by utilizing information from the observational data. Adjoint approach is one of the most widely used DA techniques. It belongs to the field of control theory, which essentially aims to control (minimize) a predefined cost function. A typical cost function comprises two parts. First, a priori part defines the departure between prior and posterior control variables (e.g., initial conditions, boundary conditions and parameters) of a model, which also takes the uncertainty in the prior control variables (background error covariance) into account. Second, an observational part quantifies the misfit between model and data, with consideration of uncertainties in observational data (data error covariance). The cost function penalizes the model-data misfit in time and space; also it is subject to our prior knowledge. The essential role of the adjoint method in data assimilation is that it calculates the gradient of the cost function with respect to model control variables using the chain rule and perturbation techniques [*Schartau et al*., 2001]. Then, an optimization algorithm (e.g., Newton method) uses such gradient to estimate the decreasing direction of the cost function. The algorithm searches along the direction and gives rise to a posterior model that is relatively more consistent with observations than a prior model. Iteratively, the cost function is minimized and the model parameters are optimized.

The adjoint approach has long been used for optimizing model parameters and estimating the sensitivity of model output with respect to model input. For example, the adjoint approach plays an important role in data assimilation of atmospheric general circulation models [*Matthew*, 1986; *Marchuk*, 1995], atmospheric air quality model [*Elbern et al*., 2000], and atmospheric chemistry transport model [*Wang et al*., 2001; *Henze et al*., 2007; *Zhang et al*., 2009]. In addition, the adjoint method has been widely used in ocean circulation models [*Marotzke et al*., 1999; *Li et al*., 2003, 2004] and in ocean biogeochemistry models [*Tjiputra et al*., 2007, 2008; *Senina et al*., 2008]. Historically, sensitivity analysis, uncertainty quantification, and model parameterization have been well explored in atmospheric and oceanic sciences by using the adjoint method. However, it is still at its early stage for applications in terrestrial ecosystem biogeochemistry modeling. There have been only a few studies using an adjoint approach in terrestrial biogeochemistry modeling studies. An example is the Carbon Cycling Data Assimilation System (CCDAS) developed for model-data fusion studies [*Kaminski et al*., 2002; *Rayner et al*., 2005; *Kaminski et al*., 2013], which combines a carbon cycle model and an atmospheric transport model as well as their adjoint models. This system helps to optimize the parameters of the carbon cycle model and to constrain terrestrial carbon fluxes.

Here we develop an adjoint version of Terrestrial Ecosystem Model (TEM) [*Zhuang et al*., 2003]. It enables the TEM to utilize multiple sources of observational data, including in situ carbon flux data and global-scale MODIS GPP products. The focus of this study is to test and validate the adjoint-TEM data assimilation framework and apply it at a site-level to estimate model parameters by assimilating in situ carbon flux data. The adjoint-TEM is also used to estimate the sensitivity of model outputs with respect to model parameters. The calculation of sensitivity with the adjoint-TEM helps to infer the optimal parameters by comparing model prediction and observational data. This study makes another significant step forward in using an adjoint approach to effectively quantify model sensitivity and improve model predictability by assimilating AmeriFlux observational NEP data.

2. Method

2.1. Overview

Adjoint code for a model could be either automatically generated using existing software, or generated manually, i.e., line-by-line. For example, the Tangent-linear and Adjoint Model Compiler (TAMC) [*Giering and Kaminski*, 1998], a software tool for generating first-order derivatives of models written in FORTRAN, has been widely used for atmospheric [*Henze et al*., 2007] and oceanic modeling [*Marotzke et al*., 1999; *Stammer et al*., 2002]. Here we manually develop the adjoint code directly from TEM model codes (where model ordinary differential equations have been discretized) with an attempt to better handle the processes in the model. The adjoint-TEM is then used to conduct the sensitivity analysis and parameter estimation (Figure 1) at three sites with different plant functional types. The sensitivity analysis helps to rank the importance of parameters in carbon flux simulations. The optimized parameters are validated at several other sites, which have the same plant functional type as the parameterization sites.

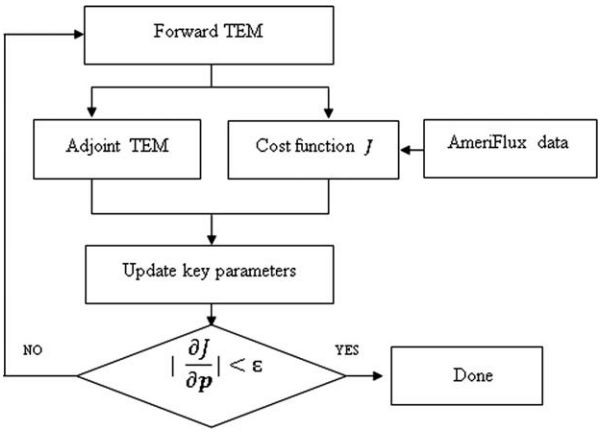

Figure 1. Flowchart of parameter optimization combining forward TEM and adjoint-TEM as well as AmeriFlux observational data.

2.2. Model and Data

The Terrestrial Ecosystem Model (TEM) [*Raich et al*., 1991; *McGuire et al*., 1992; *Melillo et al*., 1993; *Felzer et al*., 2004; *Zhuang et al*., 2001, 2002, 2003, 2010] is a process-based biogeochemistry model that uses spatially explicit data of climate, vegetation, soil, and elevation to quantify monthly fluxes of water, energy, carbon, and nitrogen in terrestrial ecosystems. TEM is constructed with a set of differential equations:

$$\frac{dC_V}{dt} = GPP - R_A - L_C \tag{1}$$

$$\frac{dC_S}{dt} = L_C - R_H \tag{2}$$

$$\frac{dN_V}{dt} = NUPTAKE - L_N \tag{3}$$

$$\frac{dN_S}{dt} = L_N - NETMIN \tag{4}$$

$$\frac{dN_{AV}}{dt} = NINPUT + NETMIN - NLOST - NUPTAKE \tag{5}$$

where $C_V, C_S, N_V, N_S, N_{AV}$ are state variables representing carbon in vegetation, soil, and detritus; nitrogen in vegetation, soil, and detritus, and available inorganic nitrogen in soil and detritus, respectively. The rest of the variables are carbon and nitrogen fluxes. $GPP, R_A, L_C, R_H, L_N, NINPUT, NETMIN, NLOST, NUPTAKE$ represent gross primary productivity, autotrophic respiration, carbon in litters, heterotrophic respiration, nitrogen in litters, nitrogen input from outside ecosystem, net rate of mineralization of N_S, nitrogen losses from ecosystem, and nitrogen uptake by vegetation, respectively. The ODEs are solved with the Runge-Kutta-Fehlberg method [*Fehlberg*, 1969], where forth-order and fifth-order Runge-Kutta solutions are compared to ensure the convergence. The whole system can be formulated as:

$$\frac{d\mathbf{y}}{dt} = f_1(\mathbf{y}, \mathbf{p}, \mathbf{c}) \tag{6}$$

where y is a vector of state variables; p and c refer to a set of parameters and initial conditions, respectively. The modeled GPP is formulated as:

$$GPP = C_{MAX} \cdot f(LEAF) \cdot f(CO_2) \cdot f(TEMP) \cdot f(PAR) \cdot f(others) \tag{7}$$

where C_{MAX} is the maximum rate of photosynthesis carbon. $f(LEAF)$ is the leaf phenology factor. $f(CO_2)$ is the atmospheric CO_2 concentration scalar factor. $f(TEMP)$ and $f(PAR)$ are the temperature and light use factors, respectively. The equation also includes several other factors. More details of the definitions of the factors can be found in previous TEM studies [*Raich et al*., 1991; *McGuire et al*., 1992; *Zhuang et al*., 2003].

The TEM is driven with monthly data of cloudiness, air temperature, and precipitation from the Climatic Research Unit [*Mitchell et al*., 2005; *New et al*., 1999, 2000, 2002]. Data of plant functional type, elevation, and soil texture (the percentages of sand, silt, and clay) are obtained from a previous study [*Zhuang et al*., 2003]. Global average atmospheric carbon dioxide concentrations data are based on observations in Mauna Loa, Hawaii [*Conway et al*., 1994; *Masarie et al*., 1995].

AmeriFlux level-4 monthly aggregated NEP data are used in this study to optimize model parameters. We focus on three typical plant functional types including grassland, deciduous broadleaf forest, and evergreen

Table 1. Description of AmeriFlux Flux Sites Used in This Study

ID	Site Name	Location	Plant Functional Type	Data Used	Reference
Calibration Sites					
1	Fort Peck	48.3°N, 105.1°W	Grassland	2000–2006	*Gilmanov et al.* [2005]
2	Bartlett Experimental Forest	44.1°N, 71.3°W	Deciduous broadleaf forest	2004–2006	*Ollinger et al.* [2005]
3	UCI_1850	55.9°N, 98.5°W	Evergreen needle-leaf forest	2002–2005	*Goulden et al.* [2006]
Extrapolation Sites					
4	Vaira Ranch	38.4°N, 120.95°W	Grassland	2001–2007	*Baldocchi et al.* [2004]
5	Fermi Prairie	41.8°N, 88.2°W	Grassland	2004–2007	*Miller et al.* [2002]
6	UMBS (Univ. of Mich. Biological Station)	45.5°N, 84.7°W	Deciduous broadleaf forest	1999–2006	*Curtis et al.* [2002]; *Schmid et al.*, [2003]
7	Missouri Ozark	38.7°N, 92.2°W	Deciduous broadleaf forest	2004–2007	*Gu et al.* [2007, 2012]
8	Wind River Crane Site	45.8°N, 121.9°W	Evergreen needle-leaf forest	1998–2002, 2004–2006	*Falk et al.* [2002]
9	Niwot Ridge	40.0°N, 105.5°W	Evergreen needle-leaf forest	1998–2007	*Turnipseed et al.* [2003, 2004]

needle-leaf forest. Nine AmeriFlux sites in the U.S. are involved in this study (Table 1). Three of them are used for sensitivity study and parameterization, and the rest are used for verification of model parameters. Specifically, at Fort Peck site [*Gilmanov et al*., 2005] 7 years data (2000–2006) are used to calibrate the grassland. Fort Peck site is in state of Montana, experiencing a cold semiarid climate with hot wet summer and cold dry winter. The optimal parameters are then extrapolated to two other grassland sites including Vaira Ranch site [*Baldocchi et al*., 2004] and Fermi Prairie site [*Miller et al*., 2002], to validate the model performance. These two sites are located in different climate zones. The Vaira Ranch site experiences a Mediterranean climate with severe acrid and high-temperature summer. The growing season occurs at cool and wet winter. The Fermi Prairie site experiences a humid continental climate with humid and hot summer and humid and cold winter. Although the environmental conditions of the three sites are distinct, the model is expected to successfully capture their seasonal carbon dynamics after we effectively calibrate the nonlinear responses of carbon fluxes to various climate variables. For deciduous broadleaf forest, the model is calibrated at Bartlett Experimental Forest site [*Ollinger et al*,. 2005] dominated by maple and beech forests, and then is extrapolated to UMBS [*Curtis et al*., 2002; *Schmid et al*., 2003] dominated by maples and oaks and Missouri Ozark [*Gu et al*., 2007, 2012] with Oak hickory forest. Although the dominant species are different, the three sites are all classified into the category of deciduous broad leaf forest according to IGBP scheme [*IGBP*, 1992]. Our model parameterization mainly focuses on calibrating processes of broadly defined plant functional types. Therefore, we ignore the species-level heterogeneity and assume that the three sites are ecologically similar. For evergreen needle-leaf forest, TEM is parameterized using 4 year data from UCI_1850 black spruce site [*Goulden et al*., 2006]. The model is then extrapolated to: (1) Wind River Crane Site [*Falk et al*., 2002], a subalpine evergreen needle-leaf forest located in state of Colorado; and (2) Niwot Ridge [*Turnipseed et al*., 2003, 2004], mainly vegetated by western hemlock with Mediterranean climate in state of Washington.

2.3. Adjoint-TEM Development

2.3.1. Cost Function

We define a cost function J to quantify the departure between the simulated and observed monthly carbon fluxes:

$$J = J_{prior} + J_{obs} \tag{8}$$

$$J_{prior} = (\mathbf{p} - \mathbf{p^o})^T \mathbf{R_p}^{-1} (\mathbf{p} - \mathbf{p^o}) \tag{9}$$

$$J_{obs} = \sum_{i=1}^{N} (\mathbf{g}_i - \mathbf{g}_i^{\mathbf{o}})^T \mathbf{R_o}^{-1} (\mathbf{g}_i - \mathbf{g}_i^{\mathbf{o}}) \tag{10}$$

where J_{prior} is the part of cost function that represents the differences between updated parameters and the prior knowledge. $\mathbf{p}$ and $\mathbf{p^o}$ are vectors of updated model parameter and prior model parameter. $\mathbf{R_p}^{-1}$ represents the inverse of the prior parameter error covariance matrix. Our prior knowledge about the parameters includes the upper and lower bounds [*Tang and Zhuang*, 2009]. We assume the variances of

prior parameters (diagonal elements of $\mathbf{R_p}$) are square of 40% of the empirical parameter ranges [*Kuppel et al*., 2012] and the correlations of prior parameters (off-diagonal elements of $\mathbf{R_p}$) are zeros. J_{obs} represents the departure between the simulated fluxes ($\mathbf{g}_i$) of interest and the observational data ($\mathbf{g}_i^0$). *N* denotes the total number of time steps over the assimilation time window. $\mathbf{R_o}^{-1}$ is the inverse of the data error covariance matrix. Traditionally, a constant data error or a fraction of the observation data is used to approximate $\mathbf{R_o}$ [*Braswell et al*., 2005; *Knorr and Kattge*, 2005]. In this study, we use 20% of the observed values (with a lower threshold of $10g \cdot C \cdot mon^{-1} \cdot m^{-2}$) as a proxy of $\mathbf{R_o}$. The relative NEP uncertainty for direct flux measurements, suggested by *Raupach et al*. [2005], ranges from 20% to 50%. Before using the observed data, we first conduct a quality control for the raw NEP data. The time series data with quality flag under 0.95 are not used in this study. Here 0.95 means 95% of the half hourly NEP data that have been used to get monthly NEP are high quality data. Because we have filtered out the uncertain data and the data used in the analysis have less uncertainty in comparison with raw data, therefore, we choose 20% to determine the uncertainty instead of the upper range of 50% in this study.

2.3.2. Adjoint Version of TEM

The adjoint-TEM is derived based on general rules of adjoint code construction [*Errico*, 1997; *Giering and Kaminski*, 1998]. The model outputs of carbon fluxes are formulated as:

$$\mathbf{g}_i = f_2(\mathbf{y}, \mathbf{p}, \mathbf{c}) \tag{11}$$

where $\mathbf{g}_i$ is the modeled carbon fluxes at the i^{th} monthly time step. $\mathbf{y}$ is a vector of state variables, $\mathbf{p}$ and $\mathbf{c}$ denote vectors of parameters and initial conditions, respectively. The adjoint-TEM will be used to calculate the sensitivity of $\mathbf{g}_i$ with respect to $\mathbf{p}$. Equation (11) can be converted into equation (12) based on adjoint method construction principles, in which the numerical algorithm for the monthly time step is treated as a sequence of operators:

$$\mathbf{g}_i = F_n\{F_{n-1}\{\cdots\{F_2\{F_1(\mathbf{y}, \mathbf{p}, \mathbf{c})\}\}\}\} \tag{12}$$

where *n* represents the number of numerical steps and $F_j (j \in [1, n])$ refers to the model operator at each numerical step.

Based on adjoint model construction principles [*Giering and Kaminski*, 1998], we define the adjoint operator $\Delta^*$with equations (13) and (14):

$$\Delta^* \mathbf{g}_i^j = \frac{\partial \mathbf{g}_i}{\partial \mathbf{g}_i^j} = \frac{\partial F_n\{F_{n-1}\{\cdots\{F_{j+1}(\mathbf{g}_i^j)\}\}\}}{\partial \mathbf{g}_i^j} \tag{13}$$

where $\mathbf{g}_i^j$ is defined as:

$$\mathbf{g}_i^j = F_j\{F_{j-1}\{\cdots\{F_2\{F_1(\mathbf{y}, \mathbf{p}, \mathbf{c})\}\}\}\}. \tag{14}$$

With the definition of equations (13) and (14), the perturbation of the TEM modeled carbon fluxes ($\Delta\mathbf{g}_i$) can be represented by an inner product of the adjoint operator $(\Delta^* \mathbf{g}_i^j)$ and the perturbation of the TEM fluxes at any numerical step *j* $(\Delta \mathbf{g}_i^j)$, which yields equations (15a) and (15b):

$$\Delta \mathbf{g}_i = < \Delta^* \mathbf{g}_i^j, \Delta \mathbf{g}_i^j > \tag{15a}$$

$$\Delta \mathbf{g}_i = < \Delta^* \mathbf{g}_i^{j-1}, \Delta \mathbf{g}_i^{j-1} > . \tag{15b}$$

Based on the first-order Taylor expansion rule, we will have equation (15c):

$$\Delta \mathbf{g}_i^j = \frac{\partial \mathbf{g}_i^j}{\partial \mathbf{g}_i^{j-1}} \cdot \Delta \mathbf{g}_i^{j-1}. \tag{15c}$$

Substituting equation (15c) into equation (15a) and apply the adjoint definition, we have equation (15d):

$$\Delta \mathbf{g}_i = < \Delta^* \mathbf{g}_i^j, \frac{\partial \mathbf{g}_i^j}{\partial \mathbf{g}_i^{j-1}} \cdot \Delta \mathbf{g}_i^{j-1} > = < \left(\frac{\partial \mathbf{g}_i^j}{\partial \mathbf{g}_i^{j-1}} \right)^T \cdot \Delta^* \mathbf{g}_i^j, \Delta \mathbf{g}_i^{j-1} > . \tag{15d}$$

By comparing equations (15d) and (15b), the operation rule of the adjoint operator Δ^* can be written as equation (16):

$$\Delta^* \mathbf{g}_i^{j-1} = \left(\frac{\partial \mathbf{g}_i^j}{\partial \mathbf{g}_i^{j-1}} \right)^T \cdot \Delta^* \mathbf{g}_i^j = (\mathbf{H}_i^j)^T \cdot \Delta^* \mathbf{g}_i^j \tag{16}$$

where $(\mathbf{H}_i^j)^T$ refers to the transpose of the Jacobian matrix. Equation (16) links the slope information during month i from numerical step j (right hand side) to numerical step $j-1$ (left hand side). We use this inverse operation rule of the adjoint operator (equation (16)) to sequentially integrate all intermediate results of transpose of the Jacobian matrix $\left(\frac{\partial \mathbf{g}_i^j}{\partial \mathbf{g}_i^{j-1}} \right)^T j \in [1, n]$ to get the gradient of the TEM output fluxes $\mathbf{g}_i$ with respect to the parameter $\mathbf{p}$:

$$\nabla_{\mathbf{p}} \mathbf{g}_i = \left(\frac{\partial \mathbf{g}_i^1}{\partial \mathbf{p}} \right)^T \cdots \left(\frac{\partial \mathbf{g}_i^j}{\partial \mathbf{g}_i^{j-1}} \right)^T \cdots \left(\frac{\partial \mathbf{g}_i^n}{\partial \mathbf{g}_i^{n-1}} \right)^T = (\mathbf{H}_i^1)^T \cdots (\mathbf{H}_i^j)^T \cdots (\mathbf{H}_i^n)^T. \tag{17}$$

Proceeding from right to left in equation (17), the order of the $\nabla_{\mathbf{p}} \mathbf{g}_i$ calculation is from the $\left(\frac{\partial \mathbf{g}_i^n}{\partial \mathbf{g}_i^{n-1}} \right)^T$ term to the $\left(\frac{\partial \mathbf{g}_i^1}{\partial \mathbf{p}} \right)^T$ term. With the help of $\nabla_{\mathbf{p}} \mathbf{g}_i$, the gradient of the cost function J with respect to model parameters $\mathbf{p}$ can be calculated as:

$$\frac{\partial J}{\partial \mathbf{p}} = \frac{\partial J_{prior}}{\partial \mathbf{p}} + \frac{\partial J_{obs}}{\partial \mathbf{p}} \tag{18a}$$

$$\frac{\partial J_{prior}}{\partial \mathbf{p}} = \mathbf{R_p}^{-1} (\mathbf{p} - \mathbf{p}^o) \tag{18b}$$

$$\frac{\partial J_{obs}}{\partial \mathbf{p}} = \sum_{i=1}^{N} \nabla_{\mathbf{p}} \mathbf{g}_i^T \cdot \mathbf{R_o}^{-1} \cdot (\mathbf{g}_i - \mathbf{g}_i^{\mathbf{o}}). \tag{18c}$$

Since the cost function J is convex, we are able to iteratively find the minimal point with optimization algorithms (section 2.5). Equation (18a) explicitly provides the optimization algorithm with necessary gradient information.

2.4. Sensitivity Study

In the sensitivity analysis, we run the model for 20 years (1989–2008) and collected the monthly model sensitivity of NEP to parameters of interest. Therefore, the analysis is based on 240 samples at each site. We conduct the sensitivity analysis at three sites representing three plant functional types including grassland (Fort Peck, 48.3°N, 105.1°W), deciduous broadleaf forest (Bartlett Experimental Forest, 44.1°N, 71.3°W), and evergreen needle-leaf forest (UCI_1850, 55.9°N, 98.5°W). Twenty-six parameters are tested in this study. These parameters are selected based on previous TEM sensitivity study [*Tang and Zhuang*, 2009] and they are associated with ecosystem processes of photosynthesis (e.g., C_{MAX}, K_I, K_C), autotrophic respiration (e.g., RA_{Q10A0}, K_R), soil respiration (e.g., RH_{Q10}, K_{DC}), nitrogen uptake (e.g., N_{MAX}), and leaf phenology (e.g., A_{LEAF}, B_{LEAF}, C_{LEAF}, MIN_{LEAF}). Detail definition and empirical ranges are documented in Table 2. The sensitivity is normalized with equation (19):

$$S_i = \frac{\frac{dg}{dp_i} \cdot \left| \frac{\sigma_{p_i}}{\sigma_g} \right|}{\sum_{j=1}^{n} \left(\left| \frac{dg}{dp_i} \cdot \frac{\sigma_{p_i}}{\sigma_g} \right| \right)} \tag{19}$$

Table 2. Twenty-Six Parameters of TEM Involved in This Study

ID	Acronym	Definition	Units	Lower Bound	Upper Bound
1	C_{MAX}	Maximum rate of photosynthesis C	g m^{-2} mon^{-1}	50	1500
2	K_I	Half saturation constant for PAR used by plants	J cm^{-2} d^{-1}	20	600
3	K_C	Half saturation constant for CO_2-C uptake by plants	μ L L^{-1}	20	600
4	T_{MAX}	Maximum temperature for GPP	°C	25	35
5	T_{MIN}	Minimum temperature for GPP	°C	−12	−1
6	T_{MAXOPT}	Maximum of optimum temperature for GPP	°C	15	25
7	A_{LEAF}	Coefficient A to model the relative photosynthetic capacity of vegetation	None	0.1	1
8	B_{LEAF}	Coefficient B to model the relative photosynthetic capacity of vegetation	None	0.1	1
9	C_{LEAF}	Coefficient C to model the relative photosynthetic capacity of vegetation	None	0	0.5
10	MIN_{LEAF}	Minimum photosynthesis capacity of vegetation	None	0.2	0.8
11	N_{MAX}	Maximum rate of N uptake by vegetation	mg m^{-2} mon^{-1}	20	700
12	K_{N1}	Half saturation constant for N uptake by vegetation	g m^{-3}	0.5	10
13	RA_{Q10A0}	Leading coefficient of the Q10 model for plant respiration	None	1.35	3.3633
14	RA_{Q10A1}	First-order coefficient of the Q10 model for plant respiration	$°C^{-1}$	−0.054577	−0.051183
15	RA_{Q10A2}	Second-order coefficient of the Q10 model for plant respiration	$°C^{-2}$	0.0022902	0.0024381
16	RA_{Q10A3}	Third-order coefficient of the Q10 model for plant respiration	$°C^{-3}$	−0.0000417	−0.0000397
17	K_{DC}	Heterotrophic respiration rate at 0°C	g g^{-1} mon^{-1}	0.0005	0.007
18	RH_{Q10}	Change in heterotrophic respiration rate due to 10°C temperature change	None	1	3
19	$MOIST_{MAX}$	Maximum soil moisture content for heterotrophic respiration	%	80	100
20	$MOIST_{MIN}$	Minimum soil moisture content for heterotrophic respiration	%	20	80
21	$MOIST_{OPT}$	Optimum soil moisture content for heterotrophic respiration	%	0	20
22	N_{UP}	Ration between N immobilized and C respired	g g^{-1}	0.005	0.1
23	K_{N2}	Half saturation constant for N uptake by organisms	g m^{-3}	0.5	1
24	C_{FALL}	Proportion of vegetation carbon loss as litter fall	g g^{-1} mon^{-1}	0.0001	0.015
25	N_{FALL}	Proportion of vegetation nitrogen loss as litter fall	g g^{-1} mon^{-1}	0.003	0.012
26	K_R	Plant respiration rate at 0°C	g g^{-1} mon^{-1}	$10^{-7.5}$	$10^{-1.5}$

where $\frac{dg}{dp_i}$ is the sensitivity of the modeled NEP with respect to a specific parameter p_i. i ranges from 1 to 26 and refers to the 26 parameters of interest. The normalized sensitivity for each parameter (S_i) is calculated by dividing the specific sensitivity by the sum of the total sensitivities. A weight factor ($|\frac{\sigma_{p_i}}{\sigma_g}|$) is used, since the values of different parameters are over a range of several orders of magnitude and the units of different parameters are usually different. σ_{p_i} is standard deviation of a specific parameter, which is defined as 40% of its empirical range; σ_g is standard deviation of modeled NEP, which is calculated from the model output of NEP time series. The original sensitivity $\frac{dg}{dp_i}$ multiplying the weight factor $|\frac{\sigma_{p_i}}{\sigma_g}|$ results in a new sensitivity value $\frac{dg}{dp_i} \cdot |\frac{\sigma_{p_i}}{\sigma_g}|$, which is a unit-less quantity. The normalized sensitivities (S_i) for different model parameters vary from -1 to 1. They are comparable, although the original values of sensitivities vary over several orders of magnitude. S_i provides a feasible ranking criteria to assess the importance of model parameters in controlling the model outputs [*Brun et al*., 2001; *Medlyn et al*., 2005].

2.5. Parameters Optimization and Uncertainty Reduction

The parameterization protocol is with the following steps (Figure 1): (1) Starting from prior estimation of parameters, we run the forward TEM to simulate carbon dynamics and also obtain all the intermediate sensitivity information $(\frac{\partial \mathbf{g}_i^j}{\partial \mathbf{g}_i^{j-1}})^T i \in [1, n1], j \in [1, n2]$ (i denotes monthly time step and j denotes numerical step during each month); (2) Use the adjoint-TEM to calculate the gradient of the model outputs of interest to parameters by integrating the intermediate sensitivities; (3) Use the simulated flux NEP, together with observational NEP to construct a cost function J; (4) Calculate sensitivity of the cost function with respect to model parameters $\left(\frac{\partial J}{\partial \mathbf{p}}\right)$ and employ optimization algorithms to minimize the cost function as well as update the model parameters; and (5) Define a constraint ε, which is a small value. In each iteration, we check if $\frac{\partial J}{\partial \mathbf{p}}$ is smaller than ε and the parameters are between the predefined empirical upper and lower bounds. If so, the model parameters are believed to be well constrained, otherwise go to step (1) and iterate the steps.

In step 4, with the help of the sensitivity of model outputs to parameters (step 2) and the definition of the cost function (step 3), we estimate the sensitivity of the cost function (J) with respect to the parameters (**p**).

Such sensitivity indicates the searching direction for parameter optimization. A Quasi-Newton method is used in this study to find the minimal point of the cost function and estimate optimal parameters:

$$\mathbf{p}_{new} = \mathbf{p}_{old} - \mathbf{d} \cdot \alpha \tag{20}$$

$$\mathbf{d} = \frac{\frac{\partial J}{\partial \mathbf{p}}}{\frac{\partial^2 J}{\partial \mathbf{p}^2}} \tag{21}$$

where $\mathbf{p}_{new}$ and $\mathbf{p}_{old}$ are updated and previous model parameters, respectively. α is the step size obtained by performing an inexact line search [*Wolfe*, 1969]. $\mathbf{d}$ is the search direction calculated by dividing gradient vector $\frac{\partial J}{\partial \mathbf{p}}$ by Hessian matrix $\frac{\partial^2 J}{\partial \mathbf{p}^2}$, where the gradient vector is explicitly calculated with equations (18a–18c) and Hessian matrix is approximated with the Broyden–Fletcher–Goldfarb–Shanno (BFGS) method [*Broyden*, 1970; *Fletcher*, 1970; *Goldfarb*, 1970; *Shanno*, 1970]. The data from eddy flux measurements at Fort Peck, Bartlett Experimental Forest and UCI_1850 sites are used to parameterize grassland, deciduous broadleaf forest and evergreen needle-leaf forest ecosystems, respectively (Table 1). The optimal parameters are extrapolated to two other sites that have the same plant functional types as the calibration sites to verify the effectiveness of the model parameterization.

The uncertainty of optimal model parameters could be calculated with the inverse of second-order derivative (or inverse covariance) at the minimal point of a cost function [*Rayner et al*., 2005; *Scholze et al*., 2007]. However, in this study the adjoint model of TEM only provides first-order derivative. Thus, we use linearity approximation (at the minimum of the cost function) to calculate posterior parameter uncertainty $(\mathbf{R}_{\mathbf{p}}^{\mathbf{post}})$ as follow [*Kaminski et al*., 2002; *Kuppel et al*., 2012]:

$$\mathbf{R}_{\mathbf{p}}^{\mathbf{post}} = \left(\sum_{i=1}^{M} \mathbf{H}_i^T \mathbf{R}_{\mathbf{o}}^{-1} \mathbf{H}_i + \mathbf{R}_{\mathbf{p}}^{-1} \right)^{-1} \tag{22}$$

where $\mathbf{R_o}$ and $\mathbf{R_p}$ are observation error covariance matrix and parameter prior error covariance matrix, respectively. $\mathbf{H}_i$ is the Jacobian matrix at the minimum of the cost function *J*. *i* starts from 1 to *M*, covering the length of assimilation time window. The uncertainty reduction is defined as: $\left(1 - \frac{\boldsymbol{\sigma}^{\mathbf{post}}}{\boldsymbol{\sigma}^{\mathbf{prior}}}\right) * 100\%$ [*Knorr and Kattge*, 2005], where $\boldsymbol{\sigma}^{\mathbf{post}}$ square root of diagonal elements from $\mathbf{R}_{\mathbf{p}}^{\mathbf{post}}$ and $\boldsymbol{\sigma}^{\mathbf{prior}}$ is 40% of prior parameter ranges.

3. Results and Discussion

3.1. Validating Adjoint Code of TEM

Developing adjoint code of TEM is a key step of this study. Before using the adjoint-TEM to optimize model parameters, we check the accuracy of the adjoint code by comparing the sensitivity calculated with adjoint-TEM with that calculated with a finite difference method.

The test simulations are carried out at the Bartlett Experimental Forest site from 2004 to 2006. By assuming local linearity, the finite difference sensitivities of NEP with respect to 26 parameters of interest are calculated:

$$\frac{\partial NEP}{\partial \mathbf{P}} = \frac{NEP(\mathbf{p} + \Delta\mathbf{p}) - NEP(\mathbf{p})}{\Delta\mathbf{p}}. \tag{23}$$

We run the forward TEM twice for each parameter, one with $\Delta\mathbf{p}$ perturbation of the parameter, the other without perturbation. $\Delta\mathbf{p} = 0.001 \cdot \mathbf{p}$ is used for all the test simulations.

Adjoint code of TEM is also used to calculate the sensitivities of NEP with respect to 26 parameters. At each numerical step, intermediate sensitivities are collected during the forward simulation. The intermediate sensitivities are then integrated by using equation (17) to calculate $\frac{\partial NEP}{\partial \mathbf{p}}$.

The adjoint-based sensitivities are fully evaluated against finite-difference-based sensitivities (Figure 2). The Pearson correlation coefficient (R^2) is 0.99993, which means that the sensitivities calculated with adjoint

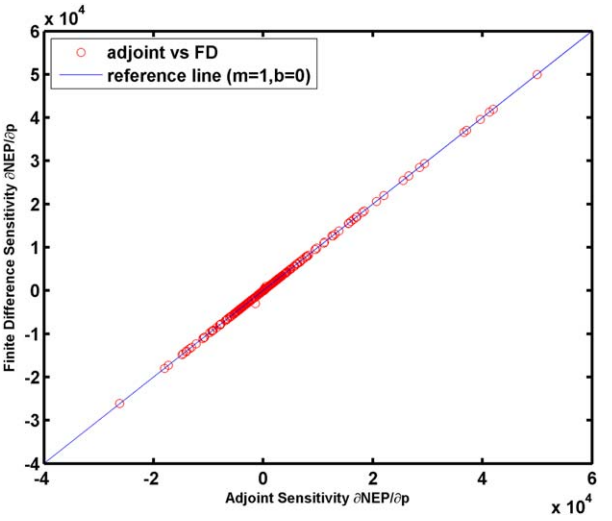

Figure 2. Validation of the adjoint code of TEM by comparing the adjoint-based sensitivity and finite difference-based sensitivity. The reference line has slope of 1 and intercept of 0.

code is consistent with those calculated with finite difference method. Thus, the accuracy of the adjoint codes of TEM is ensured.

3.2. Sensitivity Study

The sensitivity of carbon fluxes to parameters indicates the importance of model parameters in affecting carbon flux simulations. With normalization (equation (19)), the normalized sensitivities (S_i) provide insight into the relative importance of each parameter in controlling different carbon fluxes. Figures 3a–3c show the normalized sensitivity (mean value and standard deviation) of each model parameter at three different plant functional types. In Figure 3, from left to right, the parameters are ranked according to their mean S_i. Specifically, we find that: (1) C_{MAX} is the most sensitive parameter to affect NEP for all three plant functional types. The mean of the normalized $\frac{\partial NEP}{\partial C_{MAX}}$ is around 0.15, 0.15, and 0.25 for grassland, deciduous broadleaf forest, and evergreen needle-leaf forest, respectively. The standard deviations are around 0.15 at all three sites. This is consistent with the sensitivity study results using a Bayesian inference

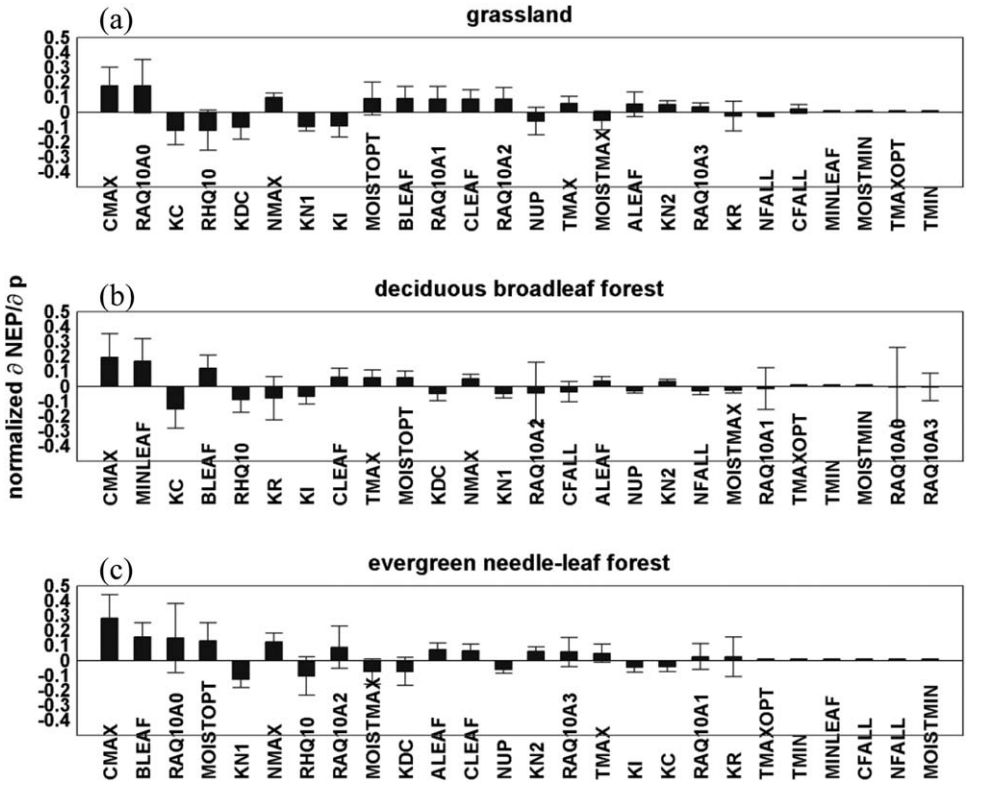

Figure 3. Normalized sensitivity of NEP with respect to 26 parameters at three sites: (a) grassland site Fort Peck; (b) deciduous broadleaf forest site Bartlett Experimental Forest; and (c) evergreen needle-leaf forest site UCI_1850. The ranking of parameters is based on the mean of their normalized sensitivities, from left (most sensitive) to right (most insensitive). Standard deviation of the sensitivity for each parameter is depicted as an error bar.

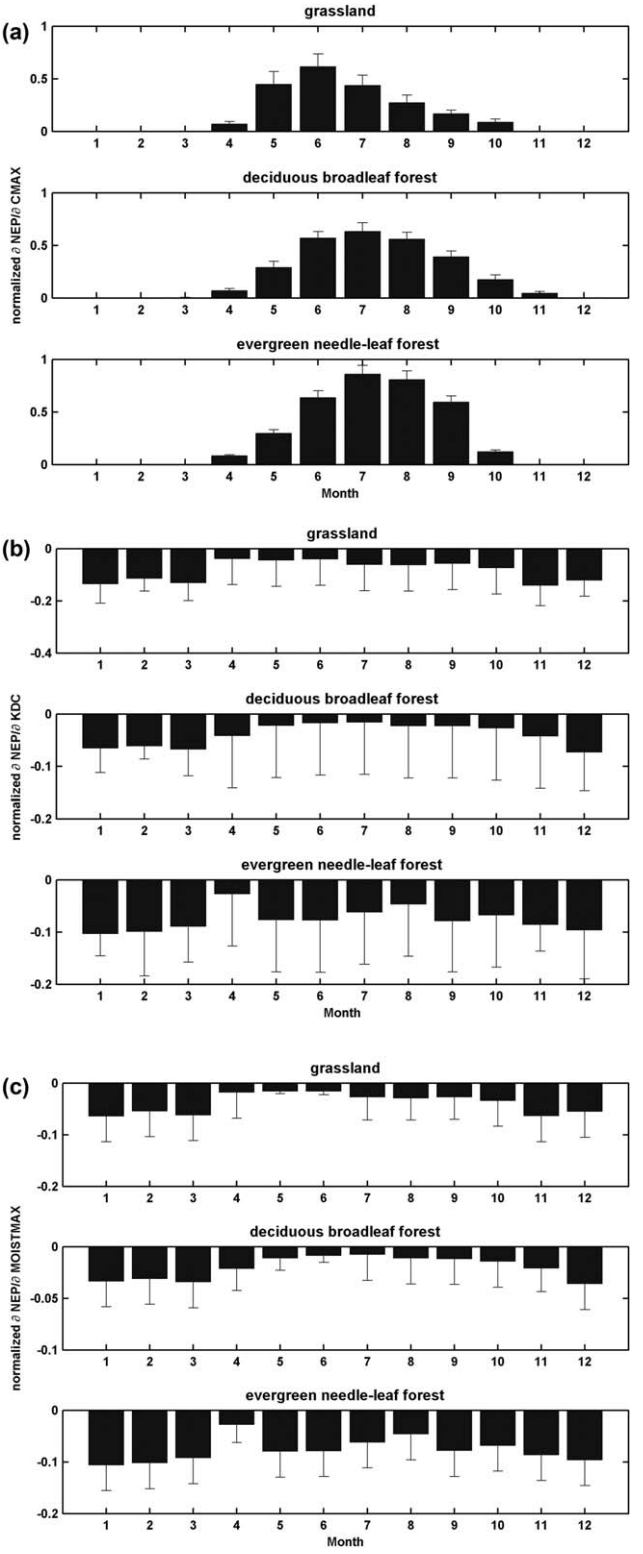

Figure 4. Seasonal variation of the normalized sensitivities of NEP to: (a) C_{MAX}, (b) K_{DC}, and (c) $MOIST_{MAX}$ at grassland, deciduous broadleaf forest and evergreen needle-leaf forest sites. C_{MAX} sensitivities are high in growing season (defined as from April to October in this study) and low in nongrowing season (defined as from December to March in this study). K_{DC} and $MOIST_{MAX}$ sensitivities, however, are relatively low in growing season and high in nongrowing season.

technique [*Tang and Zhuang*, 2009]; (2) the rankings of the other parameters' sensitivity are generally different among different sites indicating that the same ecosystem process has different degree of importance in controlling NEP for different plant functional types. For example, at deciduous forest site, two leaf parameters, MIN_{LEAF} and B_{LEAF} are ranked second and fourth, respectively. It indicates the importance of leaf phenology in modeling deciduous forest ecosystem carbon fluxes. At the grassland site, RA_{Q10A0} (plant respiration parameter) and RH_{Q10} (soil respiration parameter) are ranked second and fourth. While the ranks of leaf parameters are relatively low, which means the respirations (autotrophic and heterotrophic) are secondary dominant processes in modeling grassland carbon dynamics.

Compared with global sensitivity analysis [*Tang and Zhuang*, 2009; *Pappas et al*., 2013], adjoint sensitivity analysis provides local sensitivity knowledge over the course of simulation time window [*Cariboni et al*., 2007]. Such local sensitivities could help to understand how the model sensitivities evolve with time. Since the maximum rate of photosynthesis carbon (C_{MAX}) is the most sensitive parameter, we analyze the seasonal variation of model sensitivity to C_{MAX} (Figure 4a). The sensitivities are much higher in growing season (defined as from April to October) than those in nongrowing season (defined as from December to March). The model sensitivity to the parameter changes with time is also found in previous studies [e.g., *Prihodko et al*., 2008]. This finding is important for improving model predictability. For example, the low sensitivities in nongrowing season indicate that the ecosystem carbon budget is more affected by other factors rather than photosynthesis rate. Thus, optimizing C_{MAX} may only improve the quantification of NEP over growing season. To improve the quantification of winter NEP, other parameters should be optimized. We also find that the sensitivities of several

Table 3. Prior and Optimized Parameters for Grassland, Deciduous Broad Forest and Evergreen Needle-Leaf Forest[a]

	Grassland			Deciduous Broadleaf Forest			Evergreen Needle-Leaf Forest		
Parameters	Prior	Optimal	Uncertainty Reduction (%)	Prior	Optimal	Uncertainty Reduction (%)	Prior	Optimal	Uncertainty Reduction (%)
C_{MAX}	704.858	834.663	57.2	1352.016	1498.176	80.7	777.335	557.7487	86.2
K_I	339.5	349.2	35.8	75.47	73.8148	92.9	39.7	43.76698	91.9
K_C	442.72	403.9068	25.7	315.62	420.3171	74.5	231.96	40.71388	75.0
T_{MAX}	38	30.50582	2.8	34	34	0	34	34	0
T_{MIN}	0	0	0	0	0	0	−1	−8.97047	52.3
T_{MAXOPT}	32.7	32.7	0	30.9	30.9	0	30	30	0
A_{LEAF}	0.318	0.370962	37.5	0.863	0.895904	68.9	0.477	0.489425	6.7
B_{LEAF}	0.376	0.377533	21.3	0.362	0.378411	85.1	0.368	0.392235	58.6
C_{LEAF}	0.184	0.134152	43.3	0	0.0004	84.9	0.315	0.322962	54.8
MIN_{LEAF}	0.1	0.1	0	0.02	0.02	0	0.5	0.471896	50.2
N_{MAX}	22.746	22.74606	84.3	49.16	50.14823	95.1	21.135	596.8661	0.005
K_{N1}	0.004	0.003654	13.0	0.004	0.004158	73.4	0.004	0.002217	0.07
RA_{Q10A0}	2.357	2.040915	18.5	2.858	2.796381	67.0	2.357	1.636547	9.1
RA_{Q10A1}	−0.053	−0.05308	0.02	−0.053	−0.00217	0.3	−0.053	−0.05189	0.0007
RA_{Q10A2}	0.002	0.002384	0.01	0.003	0.002572	0.2	0.002	0.002	0
RA_{Q10A3}	-4×10^{-5}	-4×10^{-5}	0	-7×10^{-5}	-7×10^{-5}	0	-3.97×10^{-5}	-3.97×10^{-5}	0
K_{DC}	0.004	0.004144	48.6	0.006	0.004813	89.8	0.003	0.000517	24.4
RH_{Q10}	2	1.493027	36.3	2	1.805798	79.3	2	1.043601	0.1
$MOIST_{MAX}$	1	1	0	1	0.912865	34.7	1	0.811295	0.008
$MOIST_{MIN}$	0	0	0	0	0	0	0	0	0
$MOIST_{OPT}$	0.5	0.458846	30.7	0.5	0.611604	91.5	0.5	0.653863	0.5
N_{UP}	17.226	15.41427	23.0	7.03	7.00138	85.9	6.715	15.57495	0.003
K_{N2}	0.004	0.004637	3.5	0.004	0.004217	34.7	0.004	0.005323	0.0003
C_{FALL}	0.053	0.05291	0.02	0.003	0.003489	65.6	0.004	0.003429	32.8
N_{FALL}	0.032	0.03188	0.008	0.018	0.01789	4.1	0.011	0.005	0.3
K_R	0.018	0.017435	29.1	0.001	0.000741	99.5	0.002	0.003911	93.5

[a]The uncertainty reduction is defined as: $\left(1-\frac{\sigma^{post}}{\sigma^{prior}}\right) \cdot 100\%$.

soil respiration-associated parameters have strong seasonal variations. For example, the model sensitivities to K_{DC} (soil respiration rate) and $MOIST_{MAX}$ (soil moisture effect on soil respiration rate) are relatively high during nongrowing season than during growing season (Figures 4b and 4c). This indicates that soil respiration and soil moisture (rather than photosynthesis rate) dominates the nongrowing season carbon fluxes.

3.4. Parameter Optimization and Uncertainty Reduction

The prior and posterior model parameters' values are shown in Table 3. The three sets of optimized parameters are our current best estimations for grassland, deciduous broadleaf forest, and evergreen needle-leaf forest, respectively. The most sensitive parameter C_{MAX} is 834 g C mon^{-1} m^{-2} at grassland is 18% higher than its prior value. And the deciduous broadleaf forest optimal C_{MAX} (1498 g C mon^{-1} m^{-2}) is only 10% higher than the prior (1352 g C mon^{-1} m^{-2}). At needle-leaf forest site, our posterior C_{MAX} (557 g C mon^{-1} m^{-2}) is much lower (28%) than the prior value. The differences between prior and posterior model parameters indicate the change of the mean of parameter. Previous researches suggest that, in the model optimization, the change of parameter uncertainty is as important as the change of parameter value [*Raupach et al*., 2005; *Williams et al*., 2009]. Here we use the uncertainty reduction defined as $\left(1-\frac{\sigma^{post}}{\sigma^{prior}}\right) * 100\%$ to quantify the uncertainty changes of TEM model parameters.

Through data assimilation, uncertainties of prior C_{MAX} are reduced by 57%, 80%, and 86% at grassland, deciduous broadleaf forest and evergreen needle-leaf forest sites, respectively. The uncertainty reduction is lower at grassland site than the other two sites. Two other parameters associated with the plant photosynthesis are half saturation constant for CO_2 uptake by plant (K_C) and half saturation constant for photosynthetic active radiation (PAR) used by plant (K_I). We find that the uncertainty reductions of K_C and K_I are also lower at grassland site than those at forest sites (Table 3). Parameters representing the temperature effect on photosynthesis (T_{MAX}, T_{MIN} and T_{MAXOPT}) are all not well constrained by the observational data, except that uncertainty of T_{MIN} in evergreen needle-leaf forest is reduced by half. While, parameters associated with leaf phenology effects on photosynthesis (A_{LEAF}, B_{LEAF}, C_{LEAF}, and MIN_{LEAF}) are constrained relatively

well (uncertainty reduction ~21%–85%), except for A_{LEAF} at evergreen needle-leaf forest and MIN_{LEAF} at grassland and deciduous broadleaf forest.

For plant respiration process, relevant parameters are K_R and RA_{Q10A0}. The parameter K_R, representing plant respiration rate at a reference temperature, is better constrained by AmeriFlux NEP than the parameter RA_{Q10A0}, which is a Q10 factor on plant respiration. Similarly, for soil respiration, relevant parameters are K_{DC} and RH_{Q10}. We also find that the parameter K_{DC}, representing soil respiration at a reference temperature, is better constrained by observations than the Q10 factor parameter RH_{Q10}. Among different plant function types, we find that deciduous broadleaf forest's plant and soil respiration processes are best constrained (uncertainty reduction ~67%–99% for the four parameters).

The discrepancy between optima and prior parameter values and uncertainty reduction provide heuristic insights about model parameters improvement by assimilating the AmeriFlux NEP data. More importantly, uncertainty reduction will help identify the model parameters that still need to be further refined. For example, for plant nitrogen process, N_{MAX} is an important controlling parameter on NEP (Figure 3). However, using adjoint data assimilation, this parameter is not significantly improved at evergreen needle-leaf forest, with an uncertainty reduction of 0.005%, although the optimal-prior parameter discrepancy is large (575 mg N m^{-2} mon^{-1}). It means that, in order to further improve the N_{MAX} at evergreen needle-leaf forest site, extra information or more observational data are required.

3.5. Validity of the Optimized TEM

Nine AmeriFlux eddy covariance sites covering three plant functional types (grassland, deciduous broadleaf forest, and evergreen needle-leaf forest) are involved in this study. The cross-site validation approach is adapted to test the validity of the optimized TEM [*Medvigy et al*., 2009; *Verbeeck et al*., 2011]. Three sites are used for calibration; the other six sites are withheld for verification. As a result, for each plant functional type, TEM model parameters are optimized at one site and then extrapolated to two others (Table 1). To evaluate the model performance at both calibration sites and extrapolation sites, we analyzed the model-data departure at two different timescales including monthly and yearly.

Comparisons are conducted between prior, posterior model simulations and AmeriFlux observations. For monthly timescale, both prior and posterior models are able to capture the seasonality of the observed NEP (Figure 5). Generally, both models yield positive values (carbon sink) in summer and negative NEP (carbon source) in winter, except for Vaira Ranch site, due to the Mediterranean climate. The prior model is able to reasonably reproduce NEP during winter. However, in most cases, model underestimates NEP during summer (Figure 5, black lines). Moreover, there is a phase shift between prior model simulations and observations (Figure 5, black lines and blue dots). For example, at Missouri Ozark site, prior model simulations peak in April or May, while the AmeriFlux observations peak in June or July. After optimization, the posterior model is able to better reproduce the seasonal dynamics of NEP. The magnitude of carbon flux is well simulated and the phase-shift problem of the prior model is eliminated.

The improvement from the prior model simulations to the posterior model simulations is quantitatively evaluated with linear fitting statistics between prior, posterior model simulations and observational data (Table 4). The R^2 is the Pearson correlation coefficient standing for the correlations between modeled and observed flux (R^2 varies from 1 to −1, corresponding to perfectly positively and negatively correlated, respectively). A good model-data fitting will have both slope and R^2 close to 1 and intercept close to zero. We find that, at most sites, the fitting statistics between the posterior model simulations and observations are much better than those between the prior model simulations and observations. For example, at UCI_1850 evergreen needle-leaf forest site, the R^2 between prior modeled and observed NEP is improved from 0.21 to 0.80; the slope is increased from 0.9 to 0.98 and the absolute value of intercept is reduced from 9.4 to 1.3 g C mon^{-1} m^{-2}.

The posterior model is improved to different extents for various plant functional types. Specifically, the posterior model works better at the deciduous broadleaf forest sites than at the grassland and evergreen needle-leaf forest sites (Table 4). This might be due to that the model algorithm (equations (1–5)) better represents the carbon processes for deciduous forest than for grassland. For example, TEM assumes that the leaves gradually fall off from plants and enter soils. However, the plant litterfall process may not be used

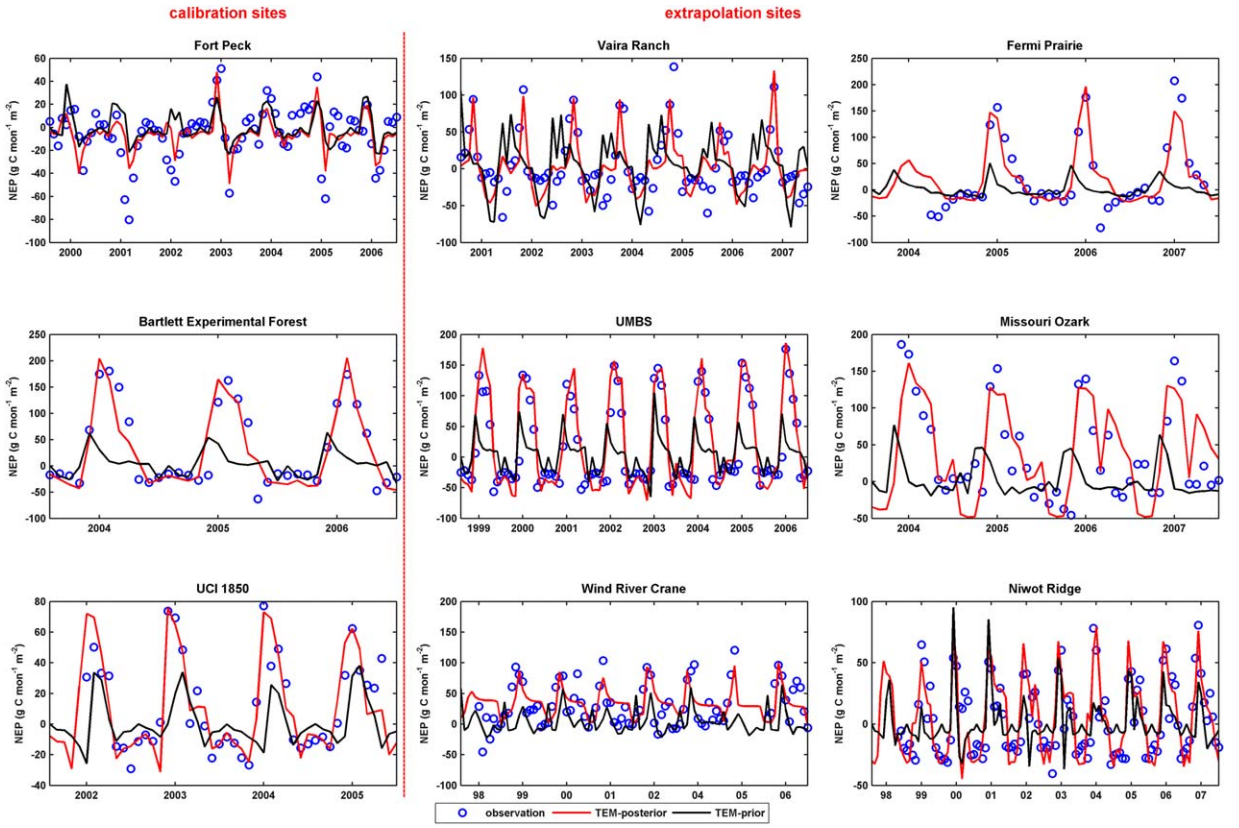

Figure 5. TEM simulated NEP by applying both prior parameters (prior-TEM) and optimized parameters (posterior-TEM) are compared with AmeriFlux NEP observations. The optimal parameters are obtained at Fort Peck, Bartlett Experimental Forest and UCI_1850 and then are extrapolated to Vaira Ranch, Fermi Prairie, UMBS, Missouri Ozark, Wind River Crane Niwot Ridge sites. The units are g C mon^{-1} m^{-2}.

appropriately to characterize the transportation of plant carbon into soil at grassland sites. Thus, in addition to using data assimilation technique to improve model parameters, revising model algorithms is also necessary to further improve model predictability [*Medlyn et al.*, 2005].

On annual timescale, the simulated carbon flux has also been significantly improved with adjoint-TEM data assimilation. In Table 5, the biases of the prior model $\left(dif1 = \frac{prior - Observation}{|Observation|} \cdot 100\%\right)$ are larger than those of the posterior model $\left(dif2 = \frac{posterior - Observation}{|Observation|} \cdot 100\%\right)$. An exception is that, at Vaira Ranch site observed annual NEP is less deviated from the prior model $(dif1 = -1.09\%)$ than from the posterior model $(dif2 = -67.50\%)$. That is because, at Vaira Ranch site, the prior TEM overestimates NEP from June to

Table 4. Model-Data Fitting Statistics (Corresponding to Figure 5) Including Slope, Interception of the Linear Regression and R^{2a}

		NEP Prior			NEP Posterior		
ID	Site Name	R^2	Slope	Intercept	R^2	Slope	Intercept
1	Fort Peck	0.16	0.75	−4.47	0.45	0.40	−3.61
2	Vaira Ranch	0.00	0.08	4.35	0.48	0.60	−1.29
3	Fermi Prairie	0.13	1.64	17.07	0.80	0.75	7.59
4	Bartlett Experimental Forest	0.16	1.28	25.59	0.83	0.90	−0.09
5	UMBS	0.20	1.04	12.47	0.82	1.04	9.24
6	Missouri Ozark	0.00	0.07	36.20	0.61	0.80	14.57
7	UCI_1850	0.21	0.90	9.40	0.80	0.98	1.30
8	Wind River Crane	0.10	0.69	26.98	0.39	0.42	21.94
9	Niwot Ridge	0.34	0.88	2.20	0.70	0.91	1.68

[a]Prior and posterior stand for model performances before and after adjoint-TEM parameter optimization, respectively.

Table 5. Mean Annual Carbon Dynamics at Calibration Sites and Extrapolation Sites[a]

ID	Site Name	NEP Prior	NEP Posterior	NEP Observation	*dif* 1 (%)	*dif* 2 (%)
1	Fort Peck	−9.30	−67.82	−60.55	84.64	−12.01
2	Vaira Ranch	55.99	18.40	56.60	−1.09	−67.50
3	Fermi Prairie	22.85	261.71	278.14	−91.78	−5.91
4	Bartlett Experimental Forest	49.90	334.48	371.13	−86.55	−9.88
5	UMBS	36.59	306.75	187.55	−80.49	63.56
6	Missouri Ozark	26.75	478.96	474.91	−94.37	0.85
7	UCI_1850	8.48	123.47	151.77	−94.42	−18.64
8	Wind River Crane	43.84	411.60	369.59	−88.14	11.37
9	Niwot Ridge	12.41	60.48	39.45	−68.54	53.30

[a]A comparison between model simulations and the observations, in which $dif1 = \frac{prior - Observation}{|Observation|} \cdot 100\%$ and $dif2 = \frac{posterior - Observation}{|Observation|} \cdot 100\%$. The units are g C yr^{-1} m^{-2}.

November and underestimates NEP from December to May (a phase shift of 4–6 months; Figure 5). The overestimation offsets the underestimation. Therefore, the prior model yields a relatively good estimation of annually aggregated NEP. Vaira Ranch grassland site is dry in summer and autumn; grass only survives during wet and warm winter and gradually becomes inactive after May [*Gretchen et al*., 2007]. The deficiency of the prior TEM to reproduce the observed seasonal variation of NEP suggests that the ecological responses of grass to extreme drought and hot climate condition may not be well represented in TEM. Overall through model data assimilation, the posterior model performance at grassland sites is improved to some extent. However, more efforts are required to further improve the model algorithm and structure for grassland ecosystems.

4. Conclusions

We develop an adjoint version of TEM and a data assimilation framework to optimize model parameters. The adjoint-TEM is used to analyze the model sensitivity to parameters and rank the importance of parameters. We find that C_{MAX} is the most important parameter in controlling net ecosystem production (NEP) for various ecosystems. The result generally agrees with the previous study using an ensemble approach [*Tang and Zhuang*, 2009]. The importance of parameters varies depending on plant functional types. We also find that the seasonality of the model sensitivity to C_{MAX} is significantly large. Typically, the sensitivity of NEP with respect to C_{MAX} is much higher during growing season than during nongrowing season. This implies that other factors, such as soil respiration parameters K_{DC} and $MOIST_{MAX}$, may play a more important role than maximum photosynthesis rate (C_{MAX}) in determining NEP during nongrowing season.

By assimilating AmeriFlux NEP data into TEM, the uncertainties of model parameters are significantly reduced and the model predictability at different timescales is improved. The model NEP simulation is improved to different degrees for various plant functional types. This suggests that, beyond parameter optimization only using NEP data, the improvement to model algorithm and structure as well as ecosystem flux data is needed. For instance, appropriate representation of litterfall process for various ecosystems will be important to improving model predictability. This study provides an effective model-data assimilation method for TEM, which would improve our future quantification of terrestrial ecosystem carbon fluxes at both site and regional levels. Our demonstration to implement an adjoint approach for ecosystem biogeochemistry modeling should also benefit the whole model-data assimilation research community.

Acknowledgments
We thank anonymous reviewers whose instructive comments help to significantly improve the quality of this paper. We acknowledge the eddy flux network principal investigators for providing carbon flux data. Ms. Jayne Piepenburg edited an earlier draft of the manuscript. This research is supported by the NASA Land Use and Land Cover Change program (NASA-NNX09AI26G), Department of Energy (DE-SC0007007), the NSF-Division of Information and Intelligent Systems (NSF-1028291), and the NSF Carbon and Water in the Earth Program (NSF-0630319).

References

Baldocchi, D. D., L. K. Xu, and N. Kiang (2004), How plant functional-type, weather, seasonal drought, and soil physical properties alter water and energy fluxes of an oak-grass savanna and an annual grassland, *Agric. For. Meteorol.*, *123*, 13–39.

Braswell, B. H., W. J. Sacks, E. Linder, and D. S. Schimel (2005), Estimating diurnal to annual ecosystem parameters by synthesis of a carbon flux model with eddy covariance net ecosystem exchange observations, *Global Change Biol.*, *11*, 335–355.

Broyden, C. G. (1970), The convergence of a class of double-rank minimization algorithms, *J. Inst. Math. Appl.*, *6*, 76–90.

Brun, R., P. Reichert, and H. R. Kunsch (2001), Practical identifiability analysis of large environmental simulation models, *Water Resour. Res.*, *37*, 1015–1030.

Cao, M., and F. Woodward (1998), Dynamic responses of terrestrial ecosystem carbon cycling to global climate change, *Nature*, *393*, 249–252.

Cariboni, J., D. Gatelli, R. Liska, and A. Saltelli (2007), The role of sensitivity analysis in ecological modelling, *Ecol. Modell.*, *203*, 167–182.

Conway, T. J., P. P. Tans, L. S. Waterman, K. W. Thoning, D. R. Kitzis, K. A. Masarie, and N. Zhang (1994), Evidence for interannual variability of the carbon cycle from the National Oceanic and#Atmospheric Administration/Climate Monitoring and Diagnostics Laboratory Global Air Sampling Network, *J. Geophys. Res.*, *99*, 22,831–22,855.

Cramer, W., D. W. Kicklighter, A. Bondeau, B. Moore III, G. Churkina, B. Nemry, A. Ruimy, and A. L. Schloss (1999), Comparing global models of terrestrial net primary productivity (NPP): Overview and key results, *Global Change Biol.*, *5*, 1–15.

Cramer, W., et al. (2001), Global response of terrestrial ecosystem structure and function to CO_2 and climate change: Results from six dynamic global vegetation models. *Global Change Biol.*, *7*, 357–373.

Curtis, P. S., P. J. Hanson, P. Bolstad, C. Barford, J. C. Randolph, H. P. Schmid, and K. B. Wilson (2002), Biometric and eddy covariance based estimates of annual carbon storage in five eastern North American deciduous forests, *Agric. For. Meteorol.*, *113*, 3–19.

Elbern, H., H. Schmidt, O. Talagrand, and A. Ebel (2000), 4D-variational data assimilation with an adjoint air quality model for emission analysis, *Environ. Modell. Software*, *15*, 539–548.

Errico, R. M. (1997), What is an adjoint model?, *Bull. Am. Meteorol. Soc.*, *78*, 2577–2591.

Falk, M., K. T. Paw U, and M. Schroeder (2002), *Long-Term Carbon and Energy Fluxes for an Old-Growth Rainforest*, 16C.2 pp., Int. Cong. of Biometeorol., Kansas City, Mo.

Fehlberg, E. (1969), Low-order classical Runge-Kutta formulas with step size control and their application to some heat transfer problems, *NASA Technical Report* 315, National Aeronautics and Space Administration, Washington D. C.

Felzer, B., D. Kicklighter, J. Melillo, C. Wang, Q. Zhuang, and R. Prinn (2004), Ozone effects on net primary production and carbon sequestration in the conterminous United States using a Biogeochemistry Model, *Tellus, Ser. B*, *56*, 230–248.

Fletcher, R. (1970), A new approach to variable metric algorithms, *Comput. J.*, *13*, 317–322.

Giering, R., and T. Kaminski (1998), Recipes for adjoint code construction, *ACM Trans. Math. Software*, *24*(4), 437–474.

Gilmanov, T. G., L. L. Tieszen, B. K. Wylie, L. B. Flanagan, A. B. Frank, M. R. Haferkamp, T. P. Meyers, and J. A. Morgan (2005), Integration of CO_2 flux and remotely-sensed data for primary production and ecosystem respiration analyses in the Northern Great Plains: Potential for quantitative spatial extrapolation, *Global Ecol. Biogeogr.*, *14*, 271–292.

Goldfarb, D. (1970), A family of variable metric updates derived by variational means, *Math. Comput.*, *24*, 23–26.

Goulden, M. L., G. C. Winston, A. M. S. McMillan, M. E. Litvak, E. L. Read, A. V. Rocha, and E. J. Rob (2006), An eddy covariance mesonet to measure the effect of forest age on land–atmosphere exchange, *Global Change Biol.*, *12*, 2146–2162, doi:10.1111/j.1365-2486.2006.01251.x.

Gretchen, M., D. Baldocchi, B. Law, and T. Meyers (2007), An analysis of soil moisture dynamics using multi-year data from a network of micrometeorological observation sites, *Adv. Water Resour.*, *30*(5), 1065–1081.

Gu, L., et al. (2007), Influences of biomass heat and biochemical energy storages on the land surface fluxes and diurnal temperature range, *J. Geophys. Res.*, *112*, D02107, doi:10.1029/2006JD007425.

Gu, L., W. J. Massman, R. Leuning, S. G. Pallardy, T. Meyers, P. J. Hanson, J. S. Riggs, K. P. Hosman, and B. Yang (2012), The fundamental equation of eddy covariance and its application in flux measurements, *Agric. For. Meteorol.*, *152*, 135–148.

Henderson-Sellers, A., A. J. Pitman, P. K. Love, P. Irannejad, and T. H. Chen (1995), The project for intercomparison of land surface parameterization schemes (PILPS): Phases 2 and 3, *Bull. Am. Meteorol. Soc.*, *76*, 489–503.

Henze, D. K., A. Hakami, and J. H. Seinfeld (2007), Development of the adjoint of GEOS-Chem, *Atmos. Chem. Phys.*, *7*, 2413–2433.

IGBP (1992), Improved global data for land applications, *IGBP Global Change Rep. 20*, edited by J. R. G. Townshend, Stockholm, Sweden.

Kaminski, T., W. Knorr, P. Rayner, and M. Heimann (2002), Assimilating atmospheric data into a terrestrial biosphere model: A case study of the seasonal cycle, *Global Biogeochem. Cycles*, *16*(4), 1066, doi:10.1029/2001GB001463.

Kaminski, T., et al. (2013), The BETHY/JSBACH Carbon Cycle Data Assimilation System: Experiences and challenges, *J. Geophys. Res. Biogeosci.*, *118*, 1414–1426, doi:10.1002/jgrg.20118.

Knorr, W., and M. Heimann (1995), Impact of drought stress and other factors on seasonal land biosphere CO_2 exchange studied through an atmospheric tracer transport model, *Tellus, Ser. B*, *47*, 471–489.

Knorr, W., and M. Heimann (2001), Uncertainties in global terrestrial biosphere modeling. 1: A comprehensive sensitivity analysis with a new photosynthesis and energy balance scheme, *Global Biogeochem. Cycles*, *15*, 207–225.

Knorr, W., and J. Kattge (2005), Inversion of terrestrial ecosystem model parameter values against eddy covariance measurements by Monte Carlo sampling, *Global Change Biol.*, *11*(8), 1333–1351.

Kuppel, S., P. Peylin, F. Chevallier, C. Bacour, F. Maignan, and A. D. Richardson (2012), Constraining a global ecosystem model with multi-site eddy-covariance data, *Biogeosciences*, *9*, 3757–3776.

Li, X., and C. Wunsch (2003), Constraining the North Atlantic circulation between 4.5°S and 39.5°N with transient tracer observations, *J. Geophys. Res.*, *108*(C10), 3318, doi:10.1029/2002JC001765.

Li, X., and C. Wunsch (2004), An adjoint sensitivity study of chlorofluorocarbons in the North Atlantic, *J. Geophys. Res.*, *109*, C01007, doi:10.1029/2003JC002014.

Limpens, J., F. Berendse, C. Blodau, J. G. Canadell, C. Freeman, J. Holden, N. Roulet, H. Rydin, and G. Schaepman-Strub (2008), Peatlands and the carbon cycle: From local processes to global implications: A synthesis, *Biogeosciences*, *5*, 1475–1491.

Luo, Y., L. White, J. Canadell, E. DeLucia, D. Ellsworth, A. Finzi, J. Lichter, and W. Shclesinger (2003), Sustainability of terrestrial carbon sequestration: A case study in Duke Forest with inversion approach, *Global Biogeochem. Cycles*, *17*(1), 1021, doi:10.1029/2002GB001923.

Luo, Y., E. Weng, X. Wu, C. Gao, X. Zhou, and L. Zhang (2009), Parameter identifiability, constraint, and equifinality in data assimilation with ecosystem models, *Ecol. Appl.*, *19*, 571–574.

Luo, Y., K. Ogle, C. Tucker, S. Fei, C. Gao, S. LaDeau, J. S. Clark, and D. S. Schimel (2011), Ecological forecasting and data assimilation in a data-rich era, *Ecol. Appl.*, *21*, 1429–1442.

Marchuk, G. I. (1995), *Adjoint Equations and Analysis of Complex Systems*, chapter 7, pp. 326–388, Springer, Dordrecht, Netherlands.

Marotzke, J., R. Giering, K. Q. Zhang, D. Stammer, C. Hill, and T. Lee (1999), Construction of the adjoint MIT ocean general circulation model and application to Atlantic heat transport sensitivity, *J. Geophys. Res.*, *104*, 29,529–29,547.

Masarie, K. A., and P. P. Tans (1995), Extension and integration of atmospheric carbon dioxide data into a globally consistent measurement record, *J. Geophys. Res.*, *100*, 11,593–11,610.

Matthew, H. (1986), Application of adjoint sensitivity theory to an atmospheric general circulation model, *J. Atmos. Sci.*, *43*, 2644–2651.

McGuire, A. D., J. M. Melillo, L. A. Joyce, D. W. Kicklighter, A. L. Grace, B. Moore III, and C. J. Vorosmarty (1992), Interactions between carbon and nitrogen dynamics in estimating net primary productivity for potential vegetation in North America, *Global Biogeochem. Cycles*, *6*, 101–124.

McGuire, A. D., et al. (2001), Carbon balance of the terrestrial biosphere in the Twentieth Century: Analyses of CO_2, climate and land use effects with four process-based ecosystem models, *Global Biogeochem. Cycles*, *15*, 183–206.

Medlyn, B., A. Robinson, R. Clement, and R. McMurtrrie (2005), On the validation of models of forest CO_2 exchanges using eddy covariance data: Some perils and pitfalls, *Tree Physiol.*, *25*, 839–857.
Medvigy, D., S. C. Wofsy, J. W. Munger, D. Y. Hollinger, and P. R. Moorcroft (2009), Mechanistic scaling of ecosystem function and dynamics in space and time: Ecosystem demography model version 2, *J. Geophys. Res.*, *114*, G01002, doi:10.1029/2008JG000812.
Melillo, J. M., A. D. McGuire, D. W. Kicklighter, B. Moore III, C. J. Vorosmarty, and A. L. Schloss (1993), Global climate change and terrestrial net primary production, *Nature*, *63*, 234–240.
Miller, R. M., S. P. Miller, J. D. Jastrow, and C. B. Rivetta (2002), Mycorrhizal mediated feedbacks influence net carbon gain and nutrient uptake in *Andropogon gerardii*, *New Phytol.*, *155*, 149–162, doi:10.1046/j.1469-8137.2002.00429.x.
Mitchell, T. D., and P. D. Jones (2005), An improved method of constructing a database of monthly climate observations and associated high-resolution grids, *Int. J. Climatol.*, *25*(6), 693–712.
Morales, P., M. T. Sykes, I. C. Prentice, P. Smith, B. Smith, H. Bugmann, and B. Zierl, et al. (2005), Comparing and evaluating process-based ecosystem model predictions of carbon and water fluxes in major European forest biomes, *Global Change Biol.*, *11*, 2211–2233.
New, M., M. Hulme, and P. D. Jones (1999), Representing twentieth century space-time climate variability. Part 1: Development of a 1961–1990 mean monthly terrestrial climatology, *J. Clim.*, *12*, 829–856.
New, M., M. Hulme, and P. D. Jones (2000), Representing twentieth century space-time climate variability. Part 2: Development of 1901–96 monthly grids of terrestrial surface climate, *J. Clim.*, *13*, 2217–2238.
New, M., D. Lister, M. Hulme, and I. Makin (2002), A high-resolution data set of surface climate over global land areas, *Clim. Res.*, *21*(1), 1–25.
Ollinger, S. V., and M. L. Smith (2005), Net primary production and canopy nitrogen in a temperate forest landscape: An analysis using imaging spectroscopy, modeling and field data, *Ecosystems*, *8*, 760–778.
Pappas, C., S. Fatichi, S. Leuzinger, A. Wolf, and P. Burlando (2013), Sensitivity analysis of a process-based ecosystem model: Pinpointing parameterization and structural issues, *J. Geophys. Res.*, *118*, 505–528, doi:10.1002/jgrg.20035.
Prihodko, L., A. S. Denning, N. P. Hanan, I. Baker, and K. Davis (2008), Sensitivity, uncertainty and time dependence of parameters in a complex land surface model, *Agric. For. Meteorol.*, *148*, 268–287.
Potter, C. S., J. T. Randerson, C. B. Field, P. A. Matson, P. M. Vitousek, H. A. Mooney, and S. A. Klooster (1993), Terrestrial ecosystem production: A process model based on global satellite and surface data, *Global Biogeochem. Cycles*, *74*, 811–841.
Raich, J. W., E. B. Rastetter, J. M. Melillo, D. W. Kicklighter, P. A. Steudler, and B. J. Peterson (1991), Potential net primary productivity in south America: Application of a global model, *Ecol. Appl.*, *1*(4), 399–429.
Raupach, M. R., P. J. Rayner, D. J. Barrett, R. S. DeFries, M. Heimann, D. S. Ojima, S. Quegan, and C. C. Schmullius (2005), Model-data synthesis in terrestrial carbon observation: Methods, data requirements and data uncertainty specifications, *Global Change Biol.*, *11*, 378–397.
Rayner, R. J., M. Scholze, W. Knorr, T. Kaminski, R. Giering, and H. Widmann (2005), Two decades of terrestrial carbon fluxes from a carbon cycle data assimilation system, *Global Biogeochem. Cycles*, *19*, GB2026, doi:10.1029/2004GB002254.
Running, S. W., and E. R. Hunt (1993), Generalization of a forest ecosystem process model for other biomes, BIOME-BGC, and an application for global-scale models, in *Scaling Physiological Processes: Leaf to Globe*, edited by J. R. Ehleringer, C. B. Field, pp. 141–158, Academic Press Inc., Waltham, Mass.
Schaefer, K., et al. (2012), A model-data comparison of gross primary productivity: Results from the North American Carbon Program site synthesis, *J. Geophys. Res.*, *117*, G03010, doi:10.1029/2012JG001960.
Schartau, M., A. Oschlies, and J. Willebrand (2001), Parameter estimates of a zero-dimensional ecosystem model applying the adjoint method, *Deep Sea Res., Part II*, *48*, 1769–1800.
Schmid, H. P., H.-B. Su, C. S. Vogel, and P. S. Curtis (2003), Ecosystem-atmosphere exchange of carbon dioxide over a mixed hardwood forest in northern lower Michigan, *J. Geophys. Res.*, *108*(D14), 4417, doi:10.1029/2002JD003011.
Scholze, M., T. Kaminski, P. Rayner, W. Knorr, and R. Giering (2007), Propagating uncertainty through prognostic carbon cycle data assimilation system simulations, *J. Geophys. Res.*, *112*, D17305, doi:10.1029/2007JD008642.
Senina, I., J. Sibert, and P. Lehodey (2008), Parameter estimation for basin-scale ecosystem-linked population models of large pelagic predators: Application to skipjack tuna, *Prog. Oceanogr.*, *78*(4), 319–335.
Shanno, D. F. (1970), Conditioning of quasi-Newton methods for function minimization, *Math. Comput.*, *24*, 647–656.
Smith, B., I. Prentice, and M. Sykes (2001), Representation of vegetation dynamics in the modeling of terrestrial ecosystems: Comparing two contrasting approaches within European climate space, *Global Ecol. Biogeogr.*, *10*, 621–637.
Stammer, D., C. Wunsch, R. Giering, C. Eckert, P. Heimbach, J. Marotzke, A. Adcroft, C. N. Hill, and J. Marshall (2002), The global ocean circulation during 1992–1997, estimated from ocean observations and a general circulation model, *J. Geophys. Res.*, *107*(C9), 3118, doi:10.1029/2001JC000888.
Tang, J., and Q. Zhuang (2009), A global sensitivity analysis and Bayesian inference framework for improving the parameter estimation and prediction of a process-based Terrestrial Ecosystem Model, *J. Geophys. Res.*, *114*, D15303, doi:10.1029/2009JD011724.
Thornton, P. E., J. F. Lamarque, N. A. Rosenbloom, and N. M. Mahowald (2007), Influence of carbon-nitrogen cycle coupling on land model response to CO_2 fertilization and climate variability, *Global Biogeochem. Cycles*, *21*, GB4018, doi:10.1029/2006GB002868.
Tjiputra, J. F., and A. M. E. Winguth (2008), Sensitivity of sea-to-air CO_2 flux to ecosystem parameters from an adjoint model, *Biogeosciences*, *5*, 615–630.
Tjiputra, J. F., D. Polzin, and A. M. E. Winguth (2007), Assimilation of seasonal chlorophyll and nutrient data into an adjoint three-dimensional ocean carbon cycle model: Sensitivity analysis and ecosystem parameter optimization, *Global Biogeochem. Cycles*, *21*, GB1001, doi:10.1029/2006GB002745.
Turnipseed, A. A., D. E. Anderson, P. D. Blanken, W. M. Baugh, and R. K. Monson (2003), Airflows and turbulent flux measurements in mountainous terrain. Part 1: Canopy and local effects, *Agric. For. Meteorol.*, *119*, 1–21.
Turnipseed, A. A., D. E. Anderson, S. Burns, P. D. Blanken, and R. K. Monson (2004), Airflows and turbulent flux measurements in mountainous terrain. Part 2: Mesoscale effects, *Agric. For. Meteorol.*, *125*, 187–205.
Verbeeck, H., P. Peylin, C. Bacour, D. Bonal, K. Steppe, and P. Ciais (2011), Seasonal patterns of CO_2 fluxes in Amazon forests: Fusion of eddy covariance data and the ORCHIDEE model, *J. Geophys. Res.*, *116*, G02018, doi:10.1029/2010JG001544.
Wang, Y., D. J. Lary, D. E. Shallcross, S. M. Hall, and J. A. Pyle (2001), A review on the use of the adjoint method in four dimensional atmospheric chemistry data assimilation, *Q. J. R. Meteorol. Soc.*, *127*, 2181–2204.
Williams, M., A. Richardson, M. Reichstein, P. Stoy, P. Peylin, H. Verbeeck, N. Carvalhais, M. Jung, D. Hollinger, and J. Kattge (2009), Improving land surface models with FLUXNET data, *Biogeosciences*, *6*, 1341–1359.
Wolfe, P. (1969), Convergence conditions for ascent methods, *SIAM Rev.*, *11*(2), 226–235.
Zaehle, S., S. Sitch, B. Smith, and F. Hatterman (2005), Effects of parameter uncertainties on the modeling of terrestrial biosphere dynamics, *Global Biogeochem. Cycles*, *19*, GB3020, doi:10.1029/2004GB002395.

Zhang, L., D. J. Jacob, M. Kopacz, D. K. Henze, K. Singh, and D. A. Jaffe (2009), Intercontinental source attribution of ozone pollution at western U.S. sites using an adjoint method, *Geophys. Res. Lett.*, *36*, L11810, doi:10.1029/2009GL037950.

Zhu, Q., and Q. Zhuang (2013a), Improving the quantification of terrestrial ecosystem carbon dynamics over the United States using an adjoint method, *Ecosphere*, *4*, 118, doi:10.1890/ES13-00058.1.

Zhu, Q., and Q. Zhuang (2013b), Influences of calibration data length and data period on model parameterization and quantification of terrestrial ecosystem carbon dynamics, *Geosci. Model Dev. Discuss.*, *6*, 6835–6865, doi:10.5194/gmdd-6-6835-2013.

Zhu, Q., and Q. Zhuang (2013c), Modeling the effects of organic nitrogen uptake by plants on the carbon cycling of boreal ecosystems, *Biogeosciences*, *10*, 7943–7955, doi:10.5194/bg-10-7943-2013.

Zhuang, Q., V. E. Romanovsky, and A. D. McGuire (2001), Incorporation of a permafrost model into a large-scale ecosystem model: Evaluation of temporal and spatial scaling issues in simulating soil thermal dynamics, *J. Geophys. Res.*, *106*, 33,649–33,670, doi:10.1029/2001JD900151.

Zhuang, Q., A. D. McGuire, K. P. O'Neil, J. W. Harden, V. E. Romanovsky, and J. Yarie (2002), Modeling the soil thermal and carbon dynamics of a fire chronosequence in interior Alaska, *J. Geophys. Res.*, *107*(D1), 8147, doi:10.1029/2001JD001244.

Zhuang, Q., et al. (2003), Carbon cycling in extratropical terrestrial ecosystems of the Northern Hemisphere during the 20th century: A modeling analysis of the influences of soil thermal dynamics, *Tellus, Ser. B*, *55*, 751–767.

Zhuang, Q., H. He, Y. Lu, L. Ji, J. Xiao, and T. Luo (2010), Carbon dynamics of terrestrial ecosystems on the Tibetan Plateau during the 20th century: An analysis with a process-based biogeochemical model, *Global Ecol. Biogeogr.*, *19*(5), 649–662.